Potential of ball milling to improve clay dispersion in nanocomposites

Perrin-Sarazin, Florence; Sepehr, Maryam; Bouaricha, Salim; Denault, Johanne

National Research Council Canada   Conseil national de recherches Canada

Canada

Potential of Ball Milling to Improve Clay Dispersion in Nanocomposites

Florence Perrin-Sarazin, Maryam Sepehr, Salim Bouaricha, Johanne Denault

Industrial Materials Institute, National Research Council Canada, Boucherville, Quebec, Canada J4B 6Y4

The preparation of exfoliated polymer nanocomposites (PNC) in nonpolar system is still preoccupying researchers in the domain. The ball milling coupled with melt-compounding was used for the preparation of polypropylene/montmorillonite PNC to evaluate the potential of ball milling in the improvement of clay dispersion. Different approaches were used for doing a preliminary ball milling of clay with or without coupling agent and of all components prior to melt-compounding. The microstructure as well as the rheological and the dynamic mechanical behaviors of the PNC compounds were characterized. The best improvements in clay dispersion were obtained by ball milling clay in the presence of other components to reduce particle agglomeration. The rheological behavior of the compounds confirmed their microstructure. The thermomechanical properties of PNC showed an enhancement in the storage modulus in the glassy and the rubbery states, independent of their microstructure. POLYM. ENG. SCI., 49:651–665, 2009. © 2009 Society of Plastics Engineers

INTRODUCTION

Since the last decade, much emphasis has been put to study polymer nanocomposites (PNC) in which the incorporation of a small amount of high aspect ratio nanoscale fillers to the polymer matrix can create significant enhancement of their properties [1, 2]. Clay has been widely used as filler in PNC because its layered structure can be exfoliated into isolated single or double 1-nm-thick platelets in the polymer matrix. Exfoliation of clay can be successfully achieved in the case of polar systems, like polyamide. However, for other common nonpolar polymers, such as polyolefins, exfoliated PNC can be hardly obtained because of the lack of natural affinity between the hydrophilic clay and the hydrophobic polymer. A coupling agent between clay and polymer is particularly required in polyolefins-based systems to achieve good clay dispersion and strong clay matrix interactions. This coupling agent usually consists of maleic anhydride-grafted polymer. In addition, the use of organoclay (i.e., inorganic clay treated with surfactant that increases the initial interlayer spacing between the clay platelets and reduces the attractive forces between them) favors further intercalation of the clay platelets by the polymer and ultimately, complete exfoliation in the matrix.

Preparation of PNC by melt-compounding technique is very popular because it implies the use of conventional polymer processing equipments, generating moderate production costs. The melt-compounding of PP/clay systems generally leads to good clay dispersion and improves intercalation of clay. However, in general, clay cannot be fully exfoliated in PP, despite the optimization of processing conditions and formulations.

Ball milling is a high-energy grinding technique widely used as a standard preparation method in powder metallurgy and also employed for clay powder preparation. High-energy milling is well known to induce several mechanochemical changes in the materials that occur at different rates. Structural modification and mechanochemical activation (change in ion-exchange capacity, catalytic activity, and dissolution) have been reported for clays, leading to great changes in their surface and colloidal properties [3, 4]. In the literature, it is recognized that high-energy milling affects the clay structure by inducing predominant delamination of the platelets at the earlier stages of degradation, breaking the platelets, and finally crushing the structure in the later stages thus leading to the structure amorphization [5–7]. The clay delamination is a crucial issue in the preparation of PNC, and as it happens during the early stage of the milling process without even drastic clay structure alteration, it makes the milling very attractive.

Very few studies dealing with the use of milling in the preparation of PNC have been reported in the literature. In some works, milling has been used to improve the dispersion of clay in PNC prepared via solution intercalation and hence their properties. Lu et al. [8] mixed montmorillonite in ketone/epoxy solution by ball milling and obtained final PNC with better dispersion and impact properties. Koo et al. [9] showed the advantage of using ball milling for mixing polyvinylpyrrolidone/montmorillonite/water suspensions to obtain nanocomposites with better optical transparency. Ball milling was also used to

initiate in situ grafting polymerization on clay particles [10]. Finally, Shao et al. [11] employed milling for direct solid-state mixing of clay with polymer before melt-compounding. The authors observed partial exfoliation and better mechanical properties for bentonite/polyamide PNC [11] and vermiculite/PP PNC [12]. Improvement of clay dispersion and the PNC properties were also reported in montmorillonite/pectin PNC prepared with ball milling [13].

In this study, the potential of ball milling was investigated as an alternative way to achieve final clay exfoliation in PP/montmorillonite PNC, by creating preliminary mechanical clay delamination prior to melt-compounding. Different formulations and conditions have been studied to show the effect of preliminary ball milling on the final microstructure, rheological and dynamic mechanical properties of PNC.

EXPERIMENTAL

Materials

The polypropylene matrix used in this study is a homopolymer Pro-fax PDC-1274 from Basell Polyolefins (M_w = 250 kg/mol, MFI = 12 g/10 min at 230°C and 2.16 kg, according to the supplier datasheet).

Two natural clays (from Southern Clay Products) were used in this work: (i) untreated montmorillonite, Cloisite Na+ (CNa+), (d_{001} = 1.2 nm); (ii) organo-modified montmorillonite, Cloisite 15A (C15A), (d_{001} = 3.2 nm, surfactant: dimethyl di(hydrogenated tallow) ammonium salt with an organic content of about 40 wt% determined by TGA).

The two maleic anhydride-grafted-PP, MA-g-PPs, used as coupling agents are as follows: (i) Epolene 43 (E43) from Eastman Chemical Company (low molecular weight, M_w = 9.1 kg/mol, high MA content = 3.8 wt%) and (ii) Polybond 3150 (P3150) from Crompton Corp. (high molecular weight, M_w ∼ 200 kg/mol, MFI = 50 g/10 min at 230°C and 2.16 kg, low MA content = 0.5 wt%, according to the supplier datasheet).

Processing

Ball milling was done using a SPEX mill. Materials in their powder form were preliminary dry-blended and 3 g of the mixture was introduced into the vial of the mill. Two large balls (diameter = 12.68 mm, weight = 8.18 g) and two small ones (diameter = 6.32 mm, weight = 1 g) were used for milling. The weight ratio of ball/material was 6.12. Two milling times of 10 and 60 min were applied. A 10-min-milling time was chosen for milling clay alone and a longer milling time of 60 min for clay in the presence of other components. Table 1 summarizes the formulations prepared by ball milling and their milling times.

The ball milled formulations were then melt-compounded in a microextruder. Microextrusion was done in

TABLE 1. Formulations (in wt%) prepared by ball milling.

Compounds	CNa+	C15A	P3150[a]	E43[b]	PP[a]	Milling time (min)
[CNa+]M10	100					10
[C15A]M10		100				10
[P3150/CNa+]M10	33		67			10
[P3150/CNa+]M60	33		67			60
[E43/CNa+]M10	33			67		10
[PP/CNa+]M60	5				95	60
[PP/C15A]M60		5			95	60
[PP/P3150/CNa+]M60	5		4		91	60
[PP/P3150/C15A]M60		5	4		91	60

[a] Used in powder form after grinding with liquid nitrogen.
[b] Used in its initial commercial powder form.

a MiniLab Micro Compounder (Thermo Haake) using a counter-rotating screw configuration with a mixing part in the middle of the screw. The compounding was performed under nitrogen atmosphere at 190°C, 100 rpm, and with a recirculation time of 2 min. From the previous work, [14], a 2-min-recirculation time was found to be the best compromise to avoid the thermomechanical degradation of the polymer and ensure optimized clay dispersion. Some of the formulations were directly compounded after milling, and the others were diluted with PP to maintain the same final clay content of 5 wt% in all compounds. Note that as C15A contains 40 wt% of surfactant, the actual mineral content of C15A-based compounds is rather 3 wt%. The compounds of PP with 4 and 10 wt% P3150 used for the rheological study were also prepared by microextrusion in the same conditions used for PNC. Table 2 presents the formulations compounded by microextrusion: (i) EX PP/P3150/CNa+ and EX PP/P3150/C15A both consist of the reference compounds for which no milling is used in the preparation; (ii) EX PP/P3150/[CNa+]M10 and EX PP/P3150/[C15A]M10 consist of compounds in which clay alone is milled before melt-compounding with other components; (iii) EX PP/[P3150/CNa+]M10, EX PP/[P3150/CNa+]M60, and EX PP/[E43/CNa+]M10 consist of compounds in which inorganic clay is milled with two parts of coupling agent prior to melt-compounding with PP. The premilling of clay with coupling agent is done on one hand, for limiting clay agglomeration caused by milling and on the other hand, for favouring better mechanochemical interaction between clay and coupling agent before incorporation of PP; and (iv) EX [PP/CNa+]M60, EX [PP/C15A]M60, EX [PP/P3150/CNa+]M60, and EX [PP/P3150/C15A]M60 consist of compounds in which all components are milled together before the final melt-processing.

Characterization

X-ray diffraction (XRD) was carried out in the Bragg-Brentano configuration, on a Bruker Discover 8 diffractometer operating at 40 kV and 40 mA, with Cu Kα radia-

TABLE 2. Formulations (in wt%) melt-compounded by microextrusion.

Compounds	CNa^+	C15A	P3150[a]	PP[a]	Milled mixture (see Table 1)
EX PP/P3150/CNa^+	5		4	91	
EX PP/P3150/C15A		5	4	91	
EX PP/P3150/$[CNa^+]_{M10}$	5 $[CNa^+]_{M10}$		4	91	
EX PP/P3150/$[C15A]_{M10}$		5 $[C15A]_{M10}$	4	91	
EX PP/$[P3150/CNa^+]_{M10}$				85	15
EX PP/$[P3150/CNa^+]_{M60}$				85	15
EX PP/$[E43/CNa^+]_{M10}$				85	15
EX $[PP/CNa^+]_{M60}$					100
EX $[PP/C15A]_{M60}$					100
EX $[PP/P3150/CNa^+]_{M60}$					100
EX $[PP/P3150/C15A]_{M60}$					100

[a] Used in powder form after grinding with liquid nitrogen.

tion. The nanocomposites specimens were injection-molded with a mini-injection machine at 200°C to induce better clay orientation for testing. Clay powders were packed in the sample holders for testing. The basal distance, d_{001}, corresponding to the interlayer spacing, was determined from Bragg's law [15]: $d_{001} = \lambda/(2\sin\theta_{001})$, where λ is the wavelength of Cu Kα radiation (1.540598 Å) and θ_{001} the diffraction angle. In addition to the calculation of d_{001}, the full width at half maximum (FWHM) and the intensity (i.e., peak height) were evaluated by performing a peak fitting. A decrease in FWHM indicates a higher degree of coherent platelets stacking (i.e., more ordered system). In the opposite, a lower degree of coherent platelets stacking (i.e., more disordered system) results in an increase of FWHM and a peak intensity loss [16].

Nitrogen adsorption analysis was done on a Flowsorb 2300 instrument to measure the specific surface area (SSA) following the Brunauer et al. [17] (BET) method. CNa^+ was tested at ambient conditions ($T = 25$°C, Relative Humidity (RH) = 75–77%, and $P = 101.86$ kPa) and also after drying at 100°C for 4 h.

Scanning electron microscope (SEM) observations were performed using a field emission gun SEM (FEG-SEM) Hitachi S-4700. Samples were polished and then chemically etched following the method of Olley and Bassett [18], before being coated with a platinum deposit for observation. The polishing and chemical etching procedures used in this work have been optimized to reveal the crystalline structure (spherulites or lamellae) of the matrix as well as the presence of the clay particles (not empty holes).

Transmission electron microscope (TEM) observations were accomplished using a JEOL JEM-2011 TEM operating at 200 kV. Cryo-ultramicrotomed thin sections of 80 nm in thickness were prepared at −100°C using a diamond knife. Both SEM and TEM observations were done in the core of the injected sample cross-sections.

Thermogravimetric analysis (TGA) was conducted on a Setaram analyzer Model TG96 from 30 to 700°C at a rate of 10°C/min under dry argon atmosphere.

Small-amplitude oscillatory shear flow experiments were conducted to assess the effect of the clay dispersion on the rheological behavior. All tests were performed in the ARES rotational rheometer, using 25-mm diameter parallel plates at $T = 200$°C under a blanket of dry nitrogen. Three types of tests were carried out: (i) the time sweep to study the thermal stability of the compounds; (ii) the strain sweep to determine their linear viscoelastic zone; and (iii) the frequency sweep. In all these cases, fresh and non-presheared compression-molded specimens with randomly oriented particles were used.

Dynamic mechanical thermal analysis (DMTA) tests were performed on Rheometrics Scientific DMTA V, using the single cantilever bending geometry. The bar specimens were compression-molded at 200°C using a Carver press and cooled at a rate of 30°C/min. Tests were conducted at a fixed frequency of 6.28 rad/s, a constant strain of 0.01%, and at a temperature range of −50 to 120°C using a ramp rate of 2°C/min. Note that the chosen test condition is always in the linear viscoelastic range for all tested materials. This range was determined for PP and PP/clay-based PNCs with 5 wt% clay.

RESULTS AND DISCUSSION

Milled Clay

Figure 1 shows the XRD patterns of the CNa^+ after 0, 10, and 60 min of ball milling. The ball milling time significantly reduces the intensities of most of the reflections and this phenomenon is attributed to the structural change of the clay. With milling time, these changes occur on clay structure in the following sequence: particle delamination and breakage, agglomeration, loss of crystallinity, and finally amorphization of the structure. A ball milling time of 10 min mainly leads to a decrease of the intensity of the (001) peak. As shown by Cícel and Kranz [5], the rapid intensity decrease of the (001) peak over
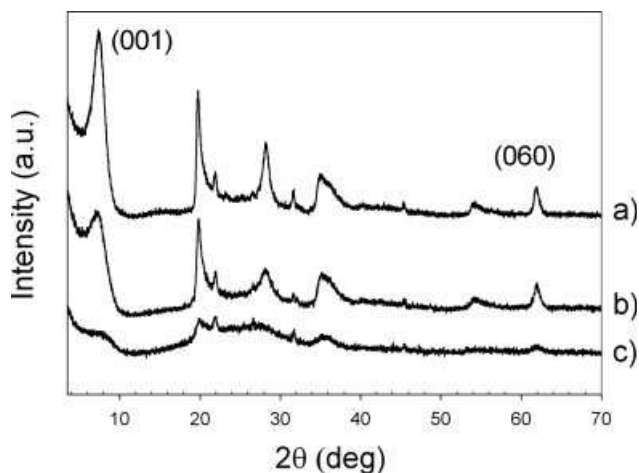
FIG. 1. XRD patterns of CNa^+ after: (a) 0, (b) 10, and (c) 60 min of ball milling.

the (060) peak indicates more dominant gliding of single or multiple platelets in the *ab* plane (i.e., platelet delamination) than platelet breakage in *ac* or *bc* planes at this stage of milling. Increasing the ball milling time to 60 min leads to more drastic change of the clay structure. A strong reduction in peak intensities is observed for both (001) and (060) peaks and, in addition, some peaks have been lost. Such a loss of crystallinity indicates that clay amorphization occurs because of the advanced degradation of the structure.

BET characterization was carried out on the CNa^+ to determine its specific surface area after different milling times. Results of the BET characterization are shown in Table 3. For both clays tested at ambient conditions or after drying, same effect on the specific surface area is observed. A milling time of 10 min leads to a significant increase of the specific surface area: +58% in the case of nondried clay and +116% in the case of dried clay. The lower increase observed for the nondried clay could be due to the presence of water adsorbed on the clay. However, a longer milling time of 60 min leads to a strong decrease of the specific surface area (see Table 3). The observed increase of the specific surface area after 10 min of milling corresponds to both delamination of the clay layered structure and breaking of the clay platelets. As the milling time increases to 60 min, agglomeration of the particles causes a decrease in the specific surface area [19, 20].

Powders of CNa^+ were observed on SEM after different ball milling times. As shown by the micrographs of Fig. 2, clay particles are in agglomerated shape and it is difficult to characterize the level of platelet delamination and breakage. However, significant differences are observed in the texture of the three samples. As the milling time increases, clay agglomerates show smaller particles with more rounded texture. This difference is more obvious by comparing nonmilled clay and 60-min-milled

clay, showing clearly the amorphization effect with milling time.

These results show that a ball milling time of 10 min for the inorganic clay CNa^+ is appropriate to induce an efficient milling without causing severe structural change. In the case of the organoclay C15A, the ball milling seems to affect the surfactant. As shown in Fig. 3a, the XRD pattern of $[C15A]_{M10}$ after 10 min of milling shows a broader (001) peak slightly shifted to larger 2θ angles, suggesting a loss of intercalation either due to the compression of the intercalated surfactant and/or its degradation during the milling. TGA analysis of C15A (Fig. 3b) reveals a small shoulder around 262°C and two typical peaks around 330 and 403°C on the derivative weight loss curve. The small shoulder is associated with the decomposition of the excess surfactant in C15A (CEC = 125 mequiv./100 g) and the two peaks with that of the intercalated surfactant [21–23]. In the case of Cloisite 20A (CEC = 95 mequiv./100 g) having the same surfactant as C15A but not in excess, this small shoulder is not present (see Fig. 3b). After milling C15A for 10 min, one observes the disappearance and decrease of the shoulder and the increase of the first peak over the second one. The calculation of the area under the derivative weight loss curves shows a very similar weight loss with slightly smaller value of loss for $[C15A]_{M10}$. The milling probably causes the loss of the excess surfactant (i.e., nonsubstituted molecules) present in the C15A. As shown in the literature [21, 22], the thermal degradation of the surfactant is highly affected by the interlayer distance. Desorption of surfactant is shown to be easier in the clay with larger interlayer spacing. After milling C15A, there is a significant decrease of the first peak and an increase of the second peak, which can be related to the smaller interlayer distance (as shown by XRD results), retarding the rate of surfactant decomposition. This is also confirmed by the similar total surfactant content determined between 150°C (after the evaporation of the water [21]) and 700°C for C15A before and after milling (≈42.5 wt%). Figure 3c presents the SEM observations done on C15A before and after 10 min of milling, showing more agglomeration in the case of $[C15A]_{M10}$. By comparing $[C15A]_{M10}$ with $[CNa^+]_{M10}$, one can note more agglomeration in the case of the former clay, indi-

TABLE 3. Results from BET characterization.

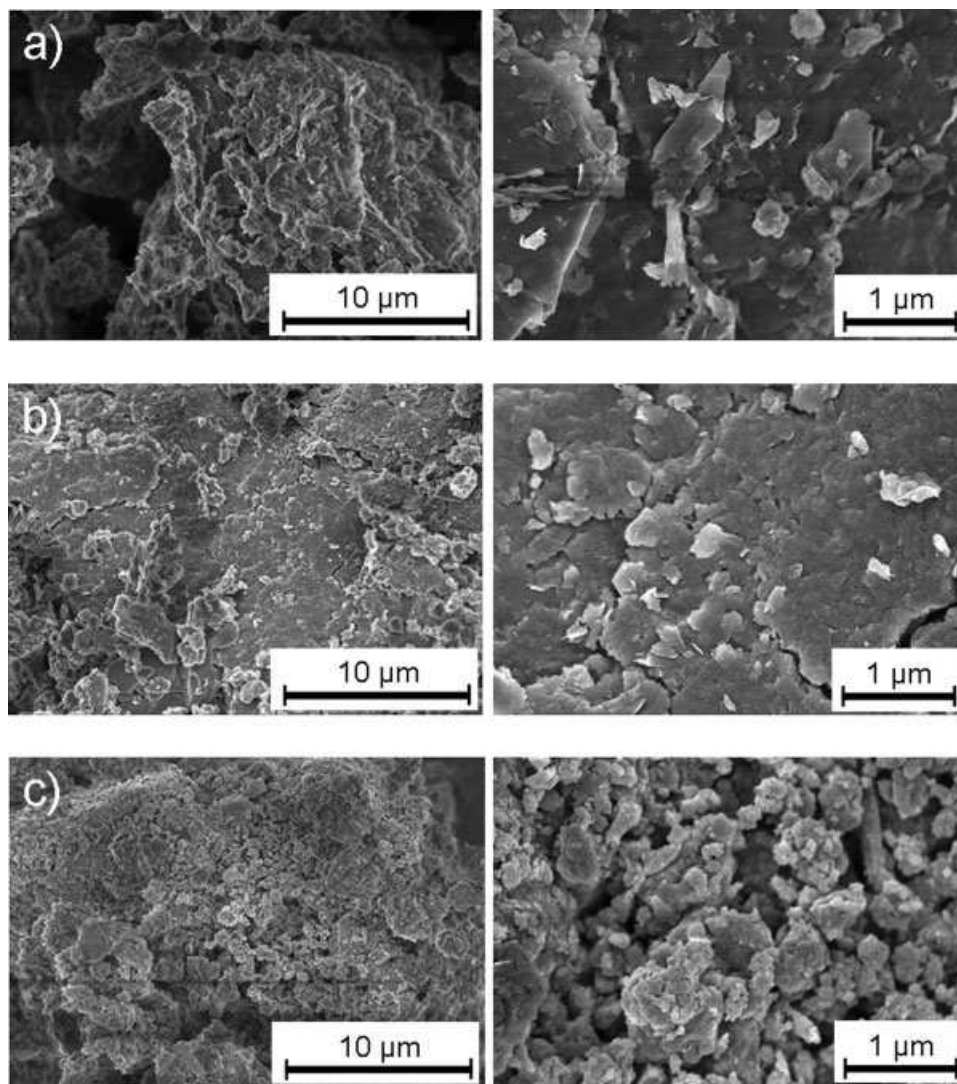| Clay CNa^+	Ball milling time (min)	Specific surface area (m²/g)	Change in SSA (%)
At ambient conditions	0	12.8	Reference
	10	20.2	+58
	60	7.5	−41
Dried (4 h at 100°C)	0	14.6	Reference
	10	31.5	+116
	60	9.4	−36

FIG. 2.   SEM micrographs of CNa^+ after: (a) 0, (b) 10, and (c) 60 min of ball milling, at magnifications of $\times 5000$ (left) and $\times 30,000$ (right).

cating the stronger effect of milling on C15A even after 10 min.

PP-PNC Prepared With Preliminary Milling

Microstructure. The XRD patterns obtained for the compounds with CNa^+ are presented in Fig. 4. The pattern of the reference formulation, EX PP/P3150/CNa^+, for which preliminary ball milling was not used, shows clearly a (001) reflection at $2\theta = 9°$ ($d_{001} = 1.0$ nm), similar to that of the dry CNa^+, indicating that melt-compounding does not affect the clay structure. The patterns of the other ball milled compounds show an obvious increase of FWHM and a decrease of the (001) peak intensity, suggesting that for most of the case, the clay structure gets disordered [16]. However, in two cases, in

addition to the peak at around $2\theta = 9°$, a small peak or shoulder is also observed at smaller angles: (i) around $2\theta = 2.5°$ ($d_{001} = 3.5$ nm), for EX PP/P3150/$[CNa^+]_{M10}$, in which clay was milled alone for 10 min; (ii) around $2\theta = 5.5°$ ($d_{001} = 1.6$ nm), for EX PP/$[E43/CNa^+]_{M10}$, in which clay was preliminary milled with E43. This suggests the presence of another degree of clay intercalation. The milling of CNa^+ alone, causing a certain amount of delaminated clay platelets, can lead to more intercalated stacks, independent of the final clay dispersion in PP. Such effect is not observed when CNa^+ is milled with others components because less clay delamination probably occurs. One exception is the case of CNa^+ milled with E43 ($M_w = 9.1$ kg/mol), in which the small molecules of the surfactant have more chance to get into the clay platelets once the latter are milled and delaminated. This is not in the case of P3150 having larger molecular
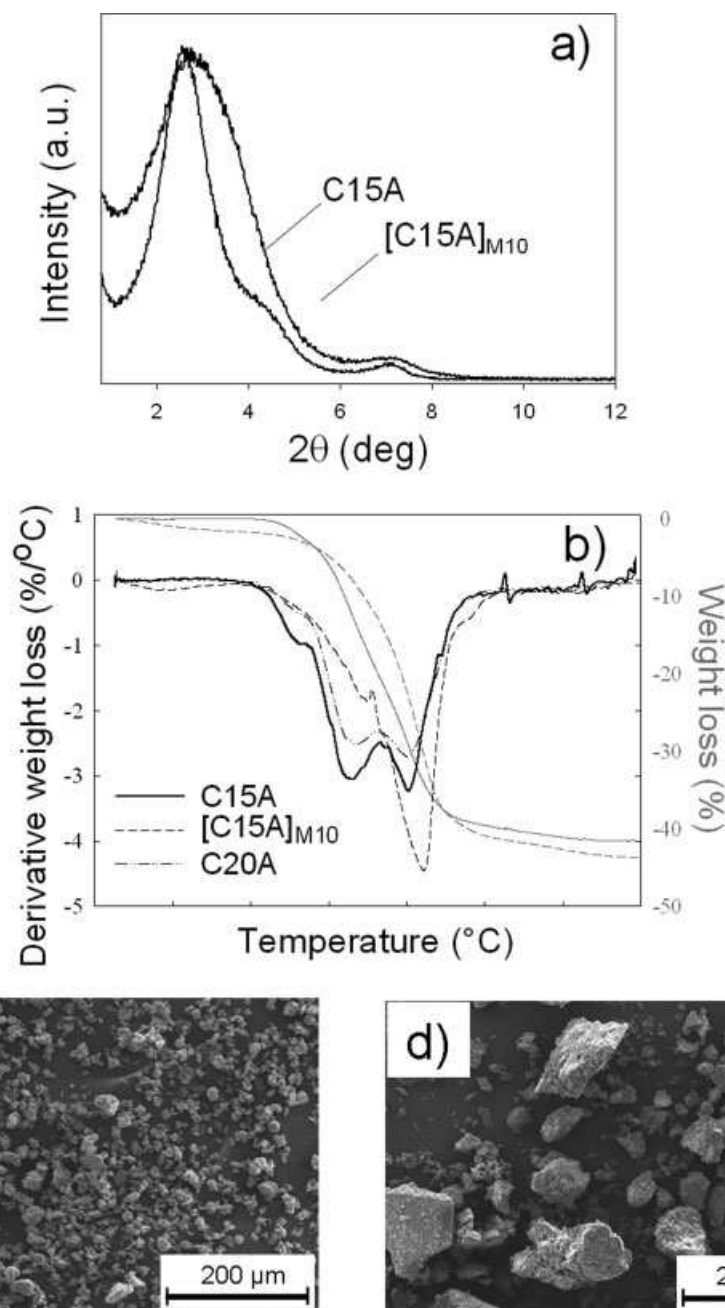
FIG. 3. The effect of milling on the organo-modified clay: (a) XRD patterns, (b) TGA scans, and SEM micrographs at ×200 magnification of C15A after 0 (c) and 10 min (d) of ball milling.

weight ($M_w \sim 200$ kg/mol). In addition, the higher amount of MA groups in E43 helps for a better interaction with clay surfaces.

The SEM micrographs presented in Figs. 5 and 7 and TEM micrographs in Figs. 6 and 8 show the clay micro and nanodispersion in the CNa^+-based compounds, respectively.

As shown by the SEM micrographs of Fig. 5a and b, both EX PP/P3150/CNa^+ (reference) and EX PP/P3150/$[CNa^+]_{M10}$ compounds have heterogeneous clay dispersion with the presence of large aggregates. The clay

microdispersion in the latter compound is not significantly affected by the preliminary milling of clay alone. The TEM observations of these two compounds (see Fig. 6) show the same low clay surface density (i.e., number of particles per area) with large aggregates having closely stacked platelets. Although a shoulder was observed at small angle on the XRD pattern of EX PP/P3150/ $[CNa^+]_{M10}$, it is difficult to confirm the presence of a higher degree of intercalation by TEM.

The SEM observations of all-milled compounds (EX $[PP/CNa^+]_{M60}$ and EX $[PP/P3150/CNa^+]_{M60}$) show signif-
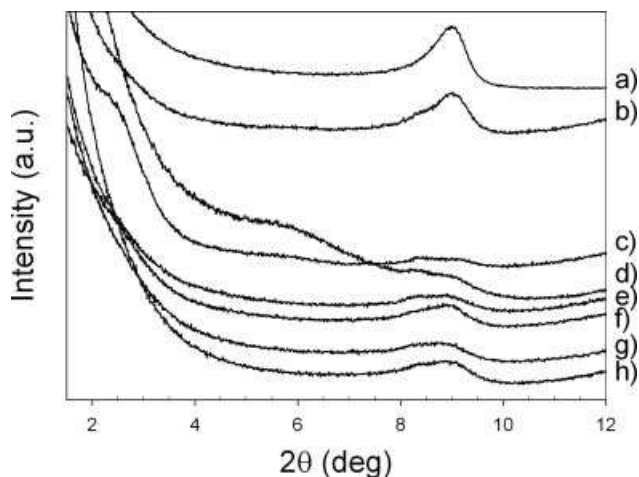
FIG. 4. XRD patterns of CNa^+-based compounds (curves have been shifted for more clarity): (a) dry CNa^+, (b) EX PP/P3150/CNa^+, (c) EX PP/P3150/[CNa^+]$_{M10}$, (d) EX PP/[E43/CNa^+]$_{M10}$, (e) EX PP/[P3150/CNa^+]$_{M10}$, (f) EX PP/[P3150/CNa^+]$_{M60}$, (g) EX [PP/CNa^+]$_{M60}$, and (h) [PP/P3150/CNa^+]$_{M60}$.

icantly finer and more homogeneous dispersion (Fig. 5c and d). This suggests that the presence of other components (i.e., PP and coupling agent) during ball milling, even for relatively long milling time, prevent CNa^+ to agglomerate. The TEM observations confirm the relatively fine clay dispersion observed by SEM in all-milled compounds, EX [PP/CNa^+]$_{M60}$ (Fig. 6c) and EX [PP/P3150/CNa^+]$_{M60}$ (Fig. 6d). These observations also show small clay aggregates composed of several short stacks of plate-lets. The presence of these short stacks indicates an important clay delamination and breakage induced by a long milling time.

SEM observations of compounds prepared with preliminary milled CNa^+ with coupling agent (see Fig. 7) show different improvements in the microdispersion depending on the type of coupling agent and the milling time. With P3150, a significant improvement of clay dispersion is observed after 60 min of milling (EX PP/[P3150/CNa^+]$_{M60}$). However, in comparison with 10-min-milled compound (EX PP/[P3150/CNa^+]$_{M10}$), a finer clay dispersion is obtained for the compound made with E43 after just 10 min of milling, confirming the XRD results. The higher reactivity of E43 (low molecular weight, high MA grafting amount) can explain this better clay dispersion obtained with this coupling agent after same milling time. Note that EX PP/[E43/CNa^+]$_{M10}$ shows some bright spherulites that are not observed in the other compounds and that are probably related to the relative high content of E43 in this formulation.

TEM observations done on EX PP/[P3150/CNa^+]$_{M10}$, EX PP/[P3150/CNa^+]$_{M60}$, and EX PP/[E43/CNa^+]$_{M10}$ (see Fig. 8), in which CNa^+ was preliminary milled with coupling agent, are also consistent with the SEM observations. Clay dispersion is greatly improved using a ball milling time of 60 min (EX PP/[P3150/CNa^+]$_{M60}$) instead of 10 min (EX PP/[P3150/CNa^+]$_{M10}$) with P3150. TEM micrographs show that clay platelets remain closely packed in EX PP/[P3150/CNa^+]$_{M60}$ with no sign of improved intercalation (Fig. 8b). In the opposite, in the case of EX PP/
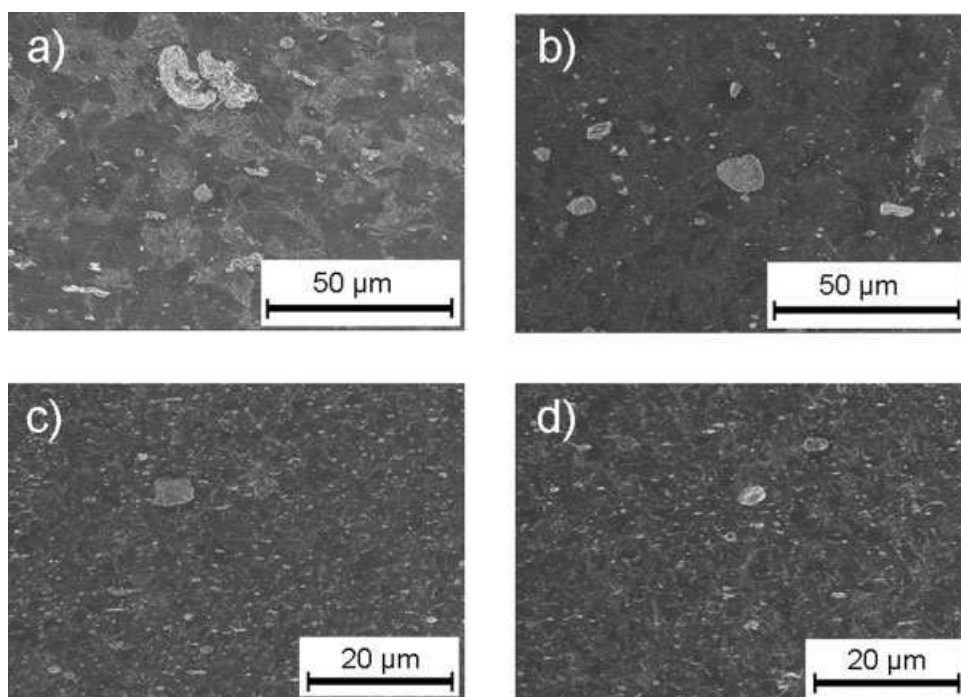

FIG. 5. SEM micrographs of CNa^+-based compounds: (a) EX PP/P3150/CNa^+ (reference) at ×1000 magnification, (b) EX PP/P3150/[CNa^+]$_{M10}$ at ×1000 magnification, (c) EX [PP/CNa^+]$_{M60}$ at ×2000 magnification, and (d) EX [PP/P3150/CNa^+]$_{M60}$, at ×2000 magnification.
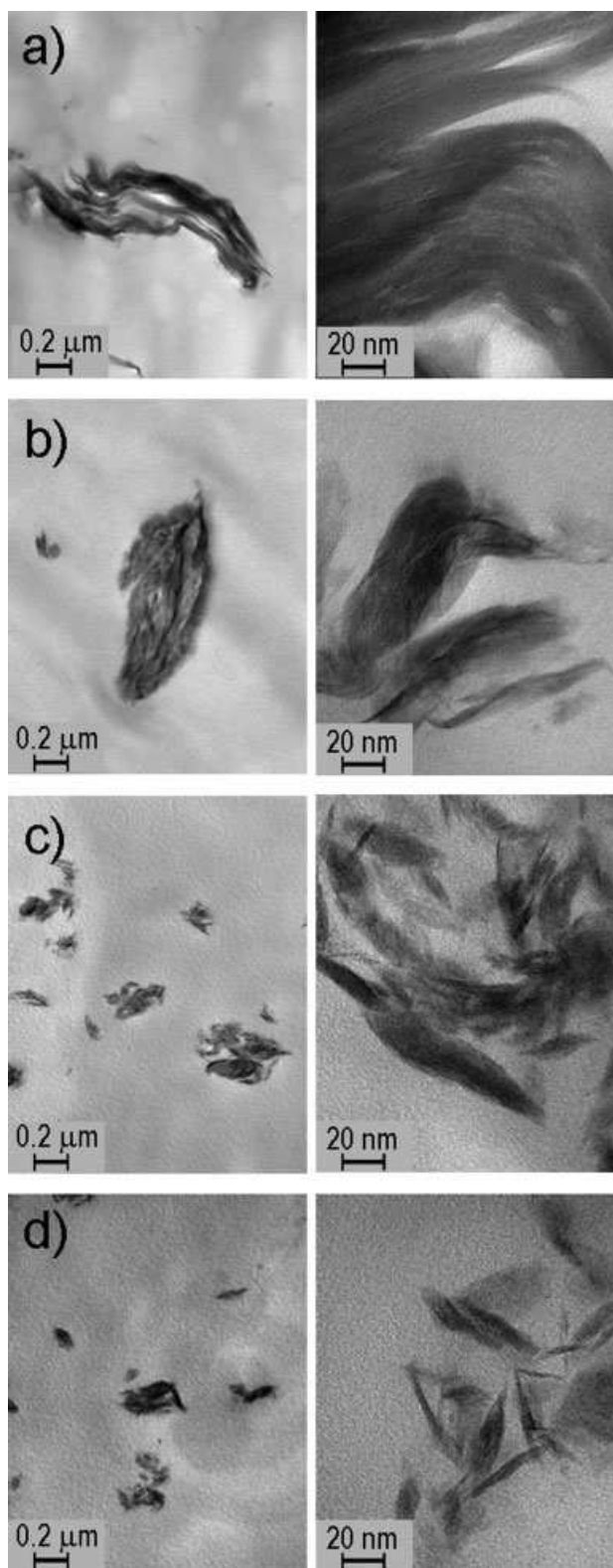
FIG. 6. TEM micrographs of CNa^+-based compounds: (a) EX PP/P3150/CNa^+, (b) EX PP/P3150/$[CNa^+]_{M10}$, (c) EX $[PP/CNa^+]_{M60}$, and (d) EX $[PP/P3150/CNa^+]_{M60}$, at TEM magnifications of $\times 50,000$ (left) and $\times 500,000$ (right).

$[E43/CNa^+]_{M10}$, clay particles are composed of small stacks with a few platelets indicating more effective delamination (Fig. 8c), and confirming the small peak observed on the XRD pattern of the EX PP/$[E43/CNa^+]_{M10}$ at small angle (see Fig. 4).

Figure 9 presents the XRD patterns of the C15A-based compounds. The pattern of reference compound, EX PP/

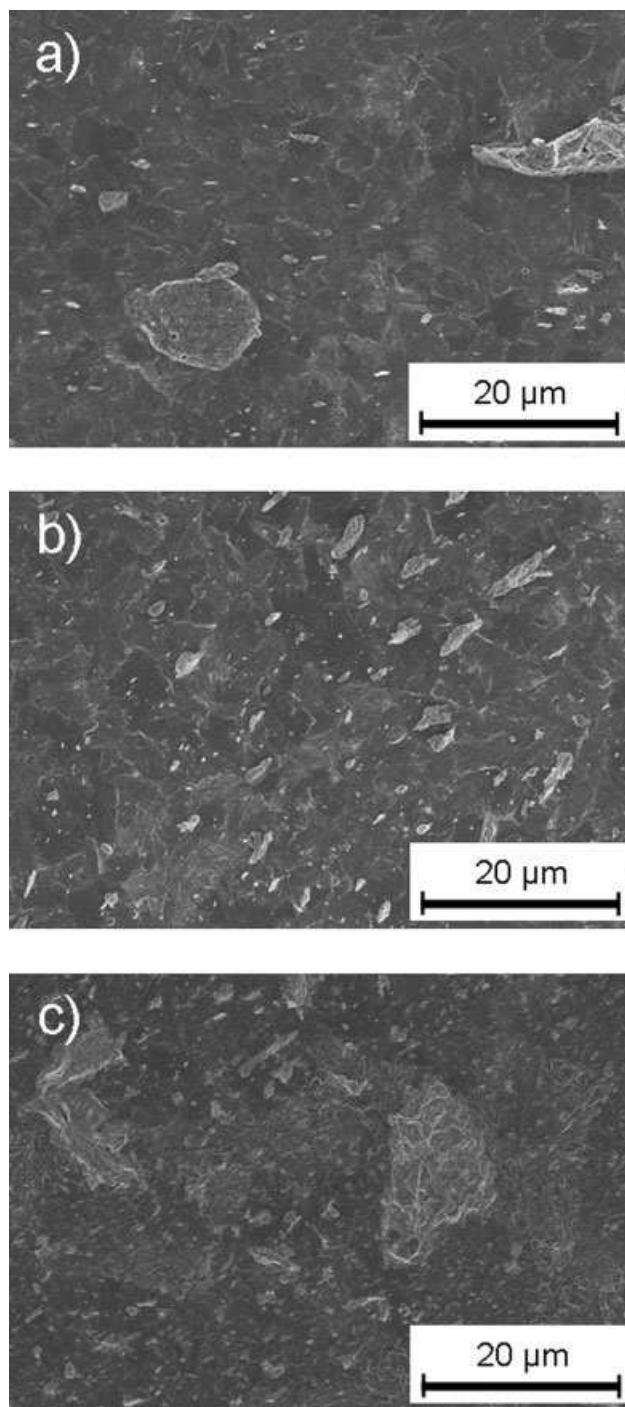FIG. 7. SEM micrographs of CNa^+-based compounds with preliminary milling of clay and coupling agent: (a) EX PP/$[P3150/CNa^+]_{M10}$, (b) EX PP/$[P3150/CNa^+]_{M60}$, and (c) EX PP/$[E43/CNa^+]_{M10}$, at $\times 2000$ magnification.
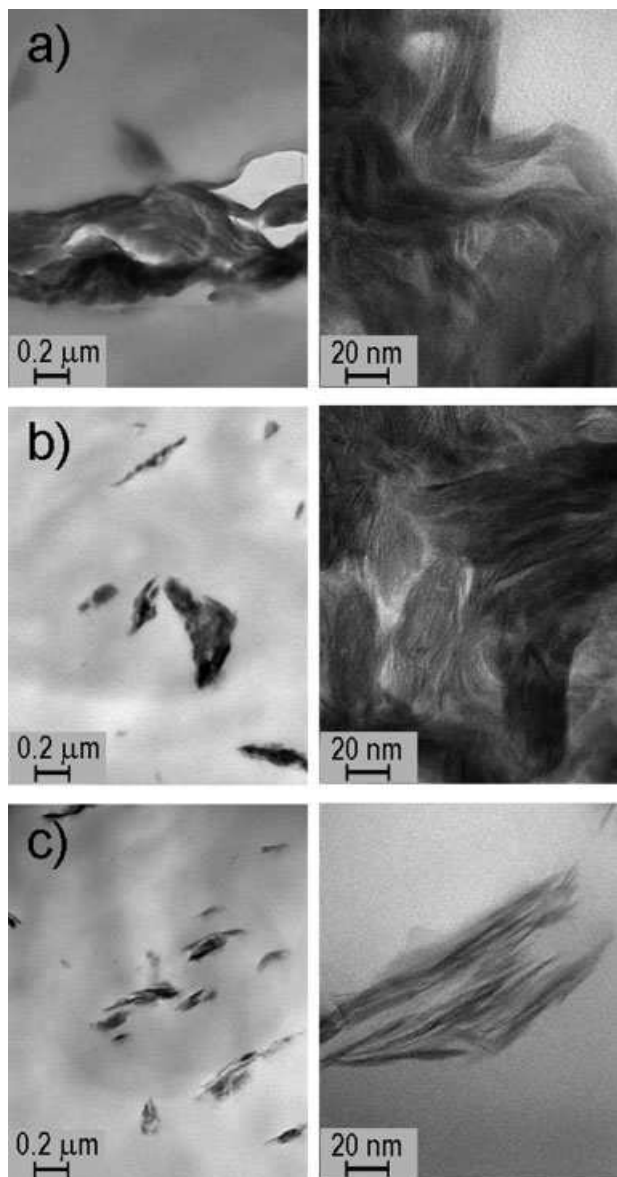
FIG. 8. TEM micrographs of CNa^+-based compounds with preliminary milling of clay and coupling agent, at two different magnifications: (a) EX PP/[P3150/CNa$^+$]$_{M10}$, (b) EX PP/[P3150/CNa$^+$]$_{M60}$, and (c) EX PP/[E43/CNa$^+$]$_{M10}$, at TEM magnifications of ×50,000 (left) and ×500,000 (right).

P3150/C15A, shows a (001) reflection located at smaller angle ($2\theta = 2.5°$, i.e., $d_{001} = 3.5$ nm) compared with that of C15A ($2\theta = 2.76°$, i.e., $d_{001} = 3.2$ nm). As expected, higher intercalation of clay is obtained in compounds with C15A, in part due to the initial higher interlayer spacing of the organoclay. As previously observed in the case of CNa^+, the patterns of all the compounds in which ball milling was used show a decrease in the intensity of the (001) peak and an increase in its FWHM. This effect is, however, more pronounced for all-milled C15A-based compounds, EX [PP/C15A]$_{M60}$ and EX [PP/P3150/C15A]$_{M60}$, than for EX PP/P3150/[C15A]$_{M10}$ in which clay was milled alone. This explains that milling C15A

for a long period of time with other components can affect more its structure than milling clay alone for a shorter period of time. Also, the large agglomeration of clay observed after milling on the [C15A]$_{M10}$ does not induce collapse of the layered structure as confirmed by the similar 2θ-position of the (001) peak for C15A and [C15A]$_{M10}$.

A simultaneous decrease in the peak intensity and 2θ-position and an increase in the FWHM value can be generally related to higher level of clay intercalation/exfoliation [16]. For EX [PP/P3150/C15A]$_{M60}$, the higher d_{001} and the asymmetry of the (001) peak when compared with EX [PP/C15A]$_{M60}$ suggest a larger degree of clay intercalation, confirming the important role of the coupling agent in the clay dispersion improvement.

The SEM micrographs presented in Fig. 10 show the clay microdispersion of the C15A-based compounds. In the case of C15A, the use of ball milling in the preparation of the compounds coarsens the clay microdispersion. As shown in Fig. 10, EX PP/P3150/[C15A]$_{M10}$ has more heterogeneous dispersion with large aggregates, when compared with EX PP/P3150/C15A. As observed earlier, ball milling affects the surfactant of C15A and leads to large agglomeration of the organoclay. Figure 10 shows poor clay microdispersion for the two all-milled compounds, EX [PP/C15A]$_{M60}$ and EX [PP/P3150/C15A]$_{M60}$. In opposite to CNa^+, the presence of other components during the milling of C15A does not help to prevent particle agglomeration.

The TEM micrographs of the compounds based on C15A are presented in Fig. 11. In agreement with the SEM, TEM observations indicate that preliminary milling of C15A leads to lower clay surface density with large particles as shown in Fig. 11b (for EX PP/P3150/[C15A]$_{M10}$) in comparison with Fig. 11a (for EX PP/P3150/C15A). This shows that, after milling C15A, the
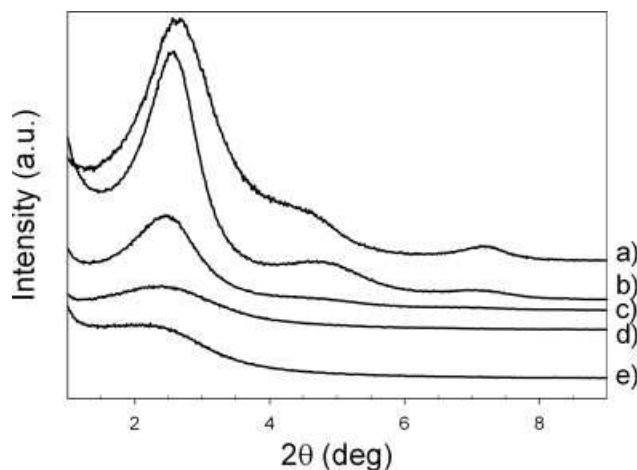

FIG. 9. XRD patterns of C15A-based compounds (curves have been shifted for more clarity): (a) dry C15A, (b) EX PP/P3150/C15A, (c) EX PP/P3150/[C15A]$_{M10}$, (d) EX [PP/C15A]$_{M60}$, and (e) EX [PP/P3150/C15A]$_{M60}$.
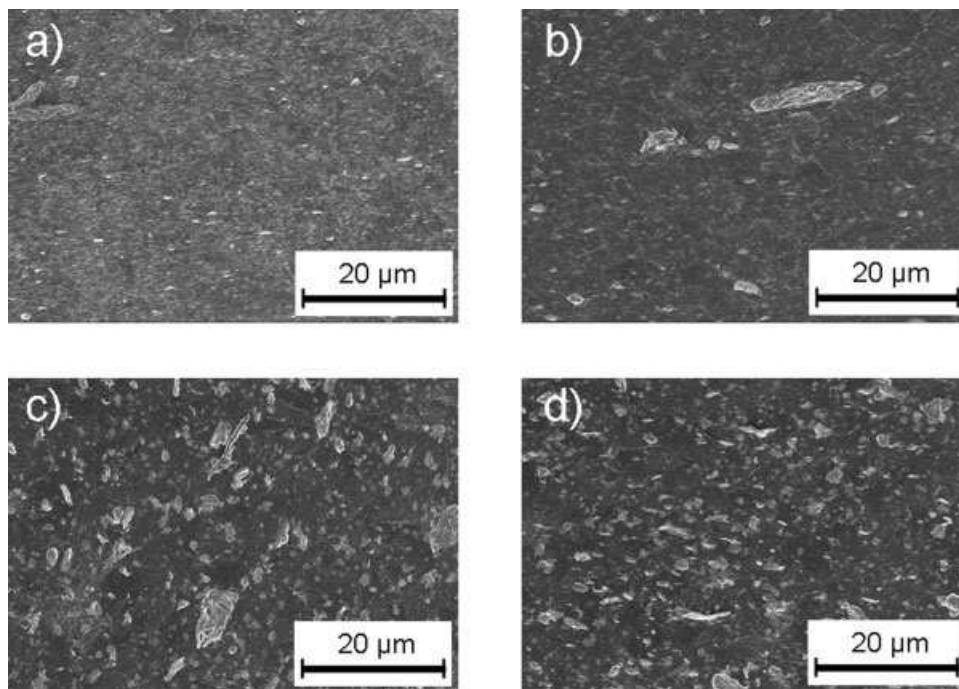
FIG. 10. SEM micrographs of C15A-based compounds: (a) EX PP/P3150/C15A (reference), (b) EX PP/P3150/[C15A]$_{M10}$, (c) EX [PP/C15A]$_{M60}$, and (d) EX [PP/P3150/C15A]$_{M60}$, at ×2000 magnification.

agglomerated particles can be hardly dispersed during melt-compounding. The TEM observations of all-milled compounds with C15A show a similar clay dispersion (Fig. 11c and d) with a clay surface density lower than that observed in EX PP/P3150/C15A but higher than that in EX PP/P3150/[C15A]$_{M10}$. The main difference resides in the organization of the clay platelets. In EX [PP/C15A]$_{M60}$ and EX [PP/P3150/C15A]$_{M60}$, clay shows a very disordered structure, which is not observed in the other compounds either with C15A or CNa$^+$. In these two compounds (Fig. 11c and d), one can often observe disordered short length platelets locally "pseudo-exfoliated" inside aggregates, indicating an extensive clay delamination coupled with breakage. As discussed earlier, the surfactant confined between the platelets is not affected by the milling and its presence lowers the surface tension of the clay platelets, probably promoting the delamination process and further intercalation. In addition, the presence of other components during milling prevents particles to agglomerate and help for better clay dispersion.

Rheology. In addition to the investigation about the processability of materials, the study of the rheological behavior of structured materials, such as polymer nanocomposites, is important for better understanding of their microstructure, particle–particle, and matrix-particle interactions. In this study, the rheological behavior of PP-based PNC prepared with or without ball milling was examined in the linear viscoelastic zone of the materials in terms of storage modulus and dynamic viscosity.

To determine the linear zone of viscoelasticity, preliminary strain sweep tests were carried out on different samples at different frequencies of $\omega = 0.628$, 6.28, and 62.8 rad/s, for shear strain of $\gamma_0 = 0.01$–1. The storage and loss moduli, G' and G'', are constant up to critical strain value, γ_c, and then decreased. Results indicate that the linear viscoelastic region of as-received PP, P3150, PP +4 wt% P3150, and EX PP/P3150/C15A, extends to $\gamma_c \cong 0.30$, 0.20, 0.20, and 0.02, respectively (the corresponding results are not shown here). All the next experiments were carried out in the linear viscoelastic zone: for PP and the coupling agent and their blends, the applied strain is 0.10 and for all compounds with 5 wt% clay, the applied strain is 0.02.

Because the rheological tests can run for a long period of time, the thermal stability of materials was checked at the temperature used for subsequent tests. Figure 12 shows the behavior of the as-received PP, P3150, PP +4 wt% P3150, PP +10 wt% P3150, and EX PP/P3150/C15A (reference compound with C15A) as a function of time at $T = 200°C$, $\omega = 6.28$ rad/s, and $\gamma_0 = 0.10$ (0.02 for EX PP/P3150/C15A). It is important to note that PP remained stable for 1 h at 200°C with a decrease of about 0.2% in dynamic viscosity and storage modulus; this decrease is about 6.8% for P3150. In the case of EX PP/P3150/C15A, PP +4 wt% P3150, and PP +10 wt% P3150, G' and η' increase about 11.1%, 14.2%, and 29.7%, respectively, during 4000 s, with a higher rate in the first 1000 s. In the case of PP + P3150, this increase in the first few hundred seconds before reaching a more stable state, represents a possible reaction between the maleic anhydride of the
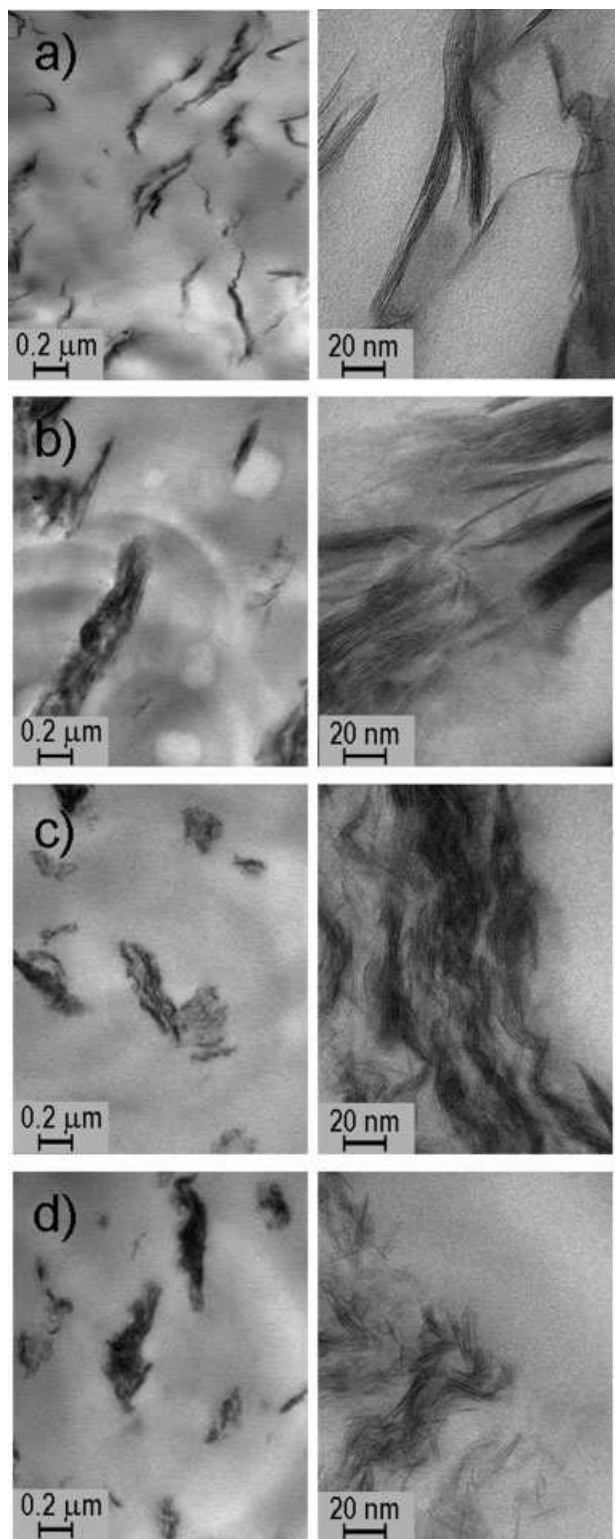
FIG. 11. TEM micrographs of C15A-based compounds at two different magnifications: (a) EX PP/P3150/C15A, (b) EX PP/P3150/[C15A]$_{M10}$, (c) EX [PP/C15A]$_{M60}$, and (d) EX [PP/P3150/C15A]$_{M60}$, at TEM magnifications of $\times$50,000 (left) and $\times$500,000 (right).

coupling agent and PP, as a partial cross linking between PP chains. During the functionalization of polyolefins via melt mixing, it is generally agreed that for isotatic polypro-

pylene, the dominant reaction is chain scission [24]. However, Rengarajan et al. [25] showed by ^{13}C NMR analysis that the grafted maleic anhydride moieties can form possible crosslinks between PP chains, explaining such increase of viscosity. The rate of increase changes with the P3150 content and the stability is reached later for high content. In the case of EX PP/P3150/C15A, a continuous increase of G' and η' suggest that a three-dimensional structure can be built in addition to the possible reaction between PP and coupling agent. G' and η' will reach a constant value even if the sample is presheared [26, 27].

The effect of processing on PP was first investigated to know how the cryo grinding and ball milling could affect the polymer. The results presented in Fig. 13 correspond to the rheological behavior of PP samples processed up to different steps. The tests were carried out at $T = 200°C$ and $\gamma_0 = 0.10$ and the scanning started at the highest fre-
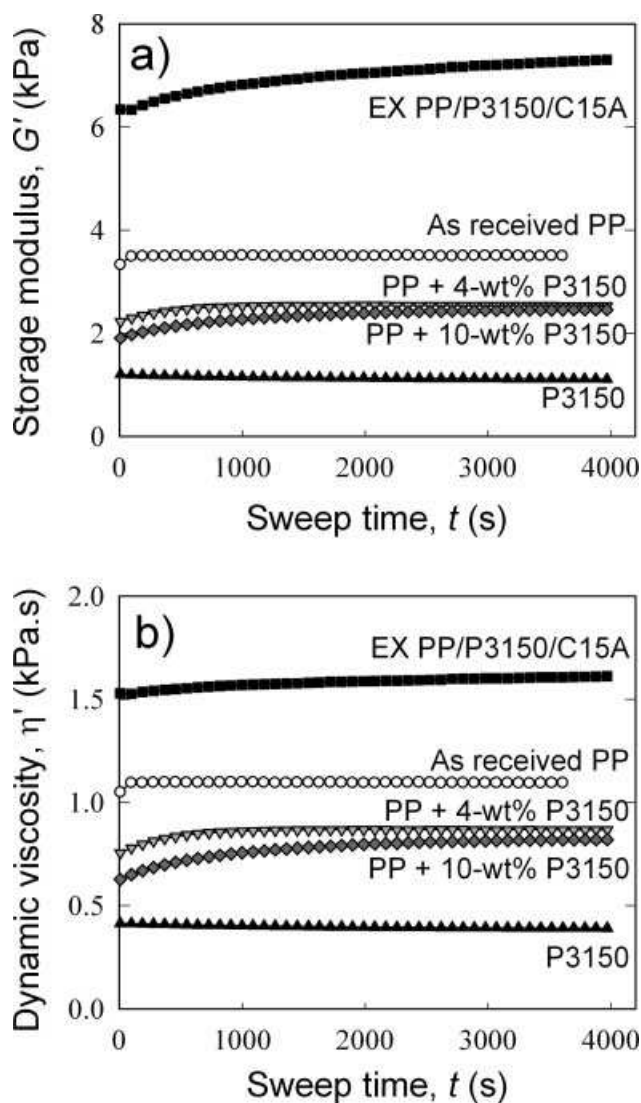

FIG. 12. Storage modulus (a), and dynamic viscosity (b) of as received PP, P3150, PP +4%-P3150, PP +10%-P3150, and EX PP/P3150/C15A as function of time, at $T = 200°C$, $\omega = 6.28$ rad/s; $\gamma_0 = 0.02$ for EX PP/P3150/C15A and $\gamma_0 = 0.10$ for all the others.
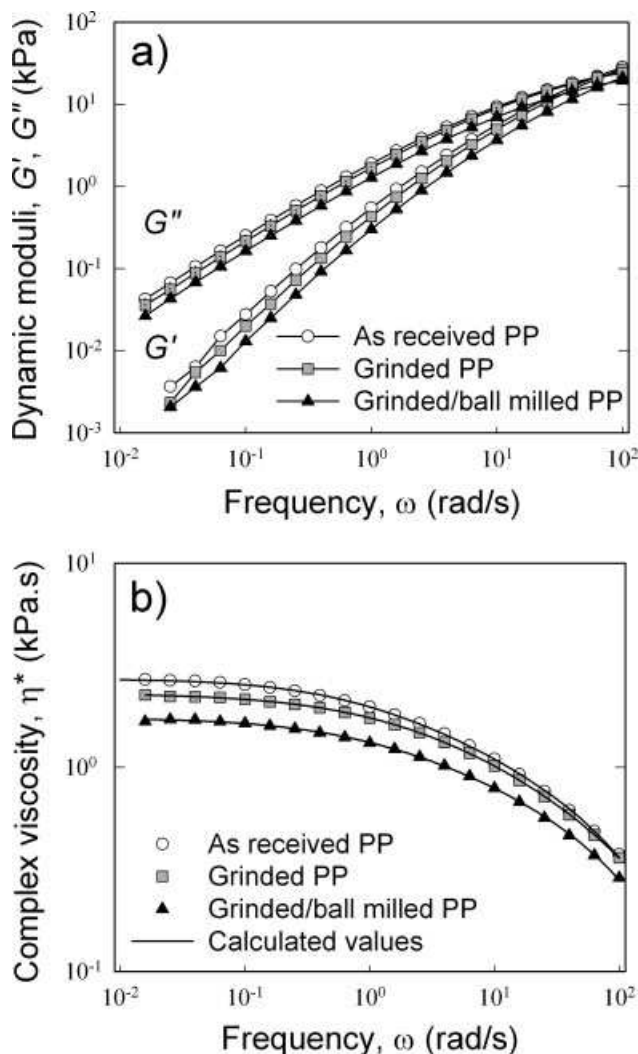
FIG. 13. Effect of processing on PP at $T = 200°C$, $\gamma_0 = 0.10$: (a) Dynamic moduli and (b) complex viscosity as a function of frequency. Symbols represent the experimental data and lines the calculated data fitted to Carreau-Yasuda equation.

quency, $\omega = 100$ rad/s. The decrease of dynamic modulus and viscosity shows that PP degraded during grinding process and even more during the ball milling. The complex viscosity of PP samples was fitted with Carreau-Yasuda model, by assuming that the Cox-Merz relation is applicable [28]:

$$\eta = \frac{\eta_0}{\left(1 + |t_1 \dot{\gamma}|^a\right)^{\frac{1-n}{a}}}$$

The parameters are zero shear viscosity, η_0, characteristic time, t_1, power law index, n and a. The obtained parameters for the PP samples, P3150, and the blends of PP and P3150 are summarized in Table 4. The zero shear viscosity decreases after each step of processing, showing the degradation of the polymer throughout the processing. The more gradual change of viscosity with the shear rate or the frequency for grinded and milled PP indicates greater molecular polydispersity or broader distribution in

molecular weight of polymer [29], which is probably a result of the scission of the polymer chains during the grinding and milling processes.

As expected, by adding the coupling agent P3150 to PP, the storage modulus and dynamic viscosity of PP decrease in respect to those of neat PP (results not shown here, the Carreau-Yasuda model parameters are summarized in Table 4). In the next figures, the behavior of PP +4 wt% P3150 was compared as matrix with that of compounds with clay.

The rheological behavior of the PNC compounds prepared with CNa^+ and C15A is shown in Figs. 14 and 15, respectively. The linear viscoelastic response of EX PP/P3150/CNa^+, EX PP/P3150/$[CNa^+]_{M10}$, and EX [PP/P3150/$CNa^+]_{M60}$, presented in Fig. 14, is similar to the blend (PP +4 wt% P3150) with a slight deviation of material functions, G' and η', at low frequencies. Similar observation of a low frequency plateau in the linear viscoelastic properties of PNC was done by Solomon et al. [30] in PP-based systems and by Ren et al. [31] in PS-based systems. Both authors associated this pseudo-solid-like behavior to the presence of a network structure built by the clay particles. It is assumed that stacks of platelets and occasionally individual platelets percolate when subjected to small-amplitude shear. By comparison with EX PP/P3150/CNa^+, the slightly higher G' shoulder of EX [PP/P3150/$CNa^+]_{M60}$, by considering the lower values at high frequencies, suggests some larger effect of the particle–particle interactions. Note that the magnitude of this shoulder is very small considering the order of measurement accuracy and can only represent a tendency of G'. This result can, however, be in relation with the finer clay dispersion and higher particle surface density observed in EX [PP/P3150/$CNa^+]_{M60}$ compared with EX PP/P3150/CNa^+ (see Fig. 6).

In the case of compounds with C15A, Fig. 15 shows a large plateau for the dynamic modulus of EX PP/P3150/C15A and a sharp increase of its dynamic viscosity at low frequencies. As mentioned earlier, such behavior is attributed to the formation of a network structure in the molten state [26, 30, 31]. In the case of exfoliated clay in polar matrix, this network structure is formed by the direct particle–particle interaction caused by percolation of the exfoliated individual platelets. However, in the case of nonpolar polymer in which coupling agent is used to

TABLE 4. Summary of obtained Carreau-Yasuda model parameters for PP, P3150, and their blends (with acceptable fitting accuracy, $R^2 = 0.999$, for all cases).

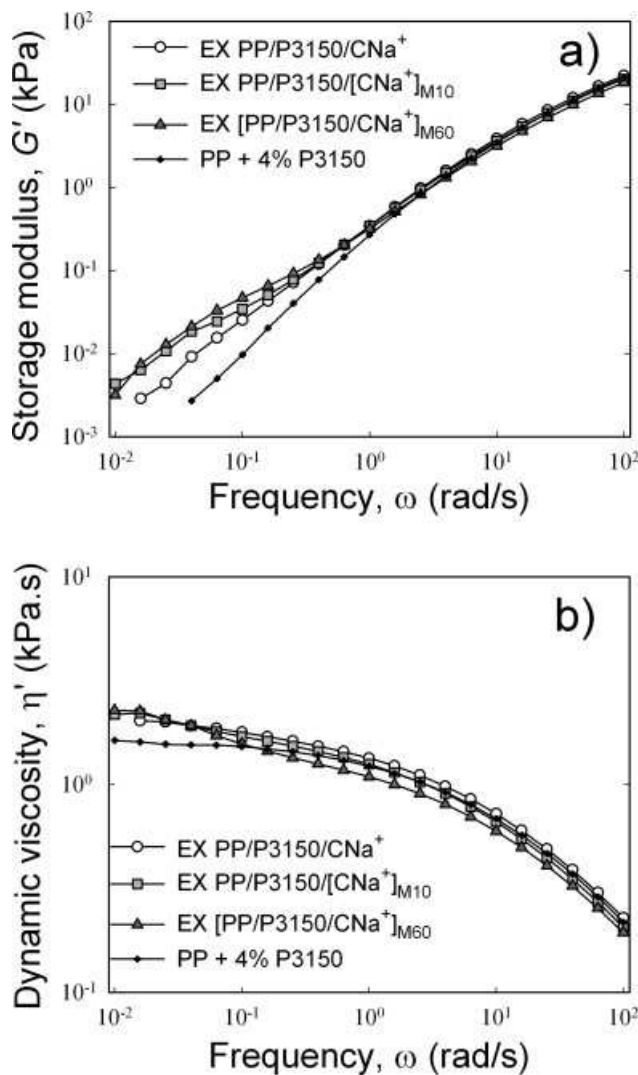| Sample	η_0 (Pa s)	t (s)	a	n
As received PP	2769	0.18	0.59	0.38
Grinded PP	2321	0.13	0.59	0.36
Grinded and ball milled PP	1777	0.09	0.55	0.33
P3150	1066	0.09	0.37	0.32
PP + 4 wt% P3150	2194	0.19	0.63	0.44
PP + 10 wt% P3150	2109	0.12	0.55	0.37

FIG. 14. Frequency sweeps at $\gamma_0 = 0.10$ and $T = 200°C$ of compounds based on PP, P3150, and CNa$^+$ made from different processing methods. (a) Dynamic modulus and (b) complex viscosity as a function of frequency.

compatibilize the polymer with clay, the built network structure is quite different. The presence of coupling agent in the compound generates multiple interactions with polymer, surfactant, and clay, and may generate microdomain structure. This complex microdomain structure coupled with the percolation effect of particles both contribute to the formation of a 3D network structure. In this case, SEM and TEM micrographs of EX PP/P3150/C15A confirm its high particle surface density in the absence of full exfoliation but a good clay dispersion with small particles of 2–20 layers per stacks. This higher particle surface density and relatively good particle-matrix interactions can then exhibit this 3D structure rheological behavior.

This is not the case for EX PP/P3150/[C15A]$_{M10}$, prepared with milled clay, which shows a very similar rheological behavior to the matrix. The absence of network

structure can be explained by the poor clay dispersion observed in this compound, resulting a low particle surface density giving less chance to particles to percolate. This also suggests that despite the presence of coupling agent, the interaction between the matrix and preliminary milled C15A remains relatively poor and comparable with the compounds based on CNa$^+$, confirming the loss of surfactant in milled C15A.

In the case of EX [PP/C15A]$_{M60}$ and EX [PP/P3150/C15A]$_{M60}$ compounds, identical rheological behaviors are observed. For clarity, the results of EX [PP/C15A]$_{M60}$ are not shown in Fig. 15. A small plateau of G' and increase of η' detected at low frequencies indicate the presence of some network structure that can be due to the contact between large particles with looser and disordered platelets as shown by the TEM micrographs of these two compounds (see Fig. 11). This reveals that the coupling agent with large molecular weight and low MA content is not
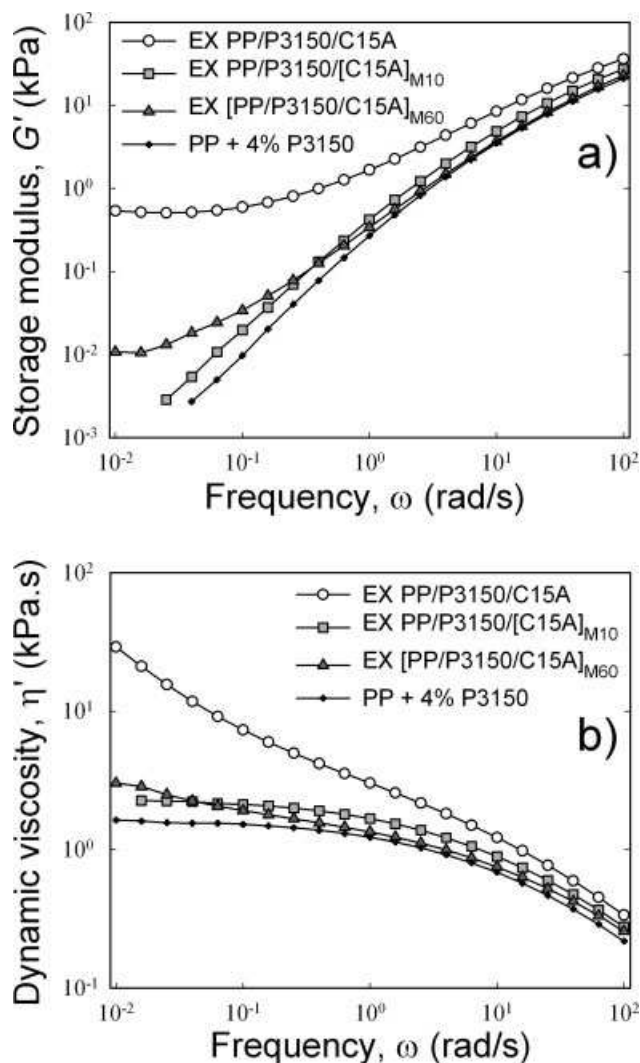

FIG. 15. Frequency sweeps at $\gamma_0 = 0.10$ and $T = 200°C$ of compounds based on PP, P3150 and C15A made from different processing methods. (a) Dynamic modulus and (b) complex viscosity as a function of frequency.
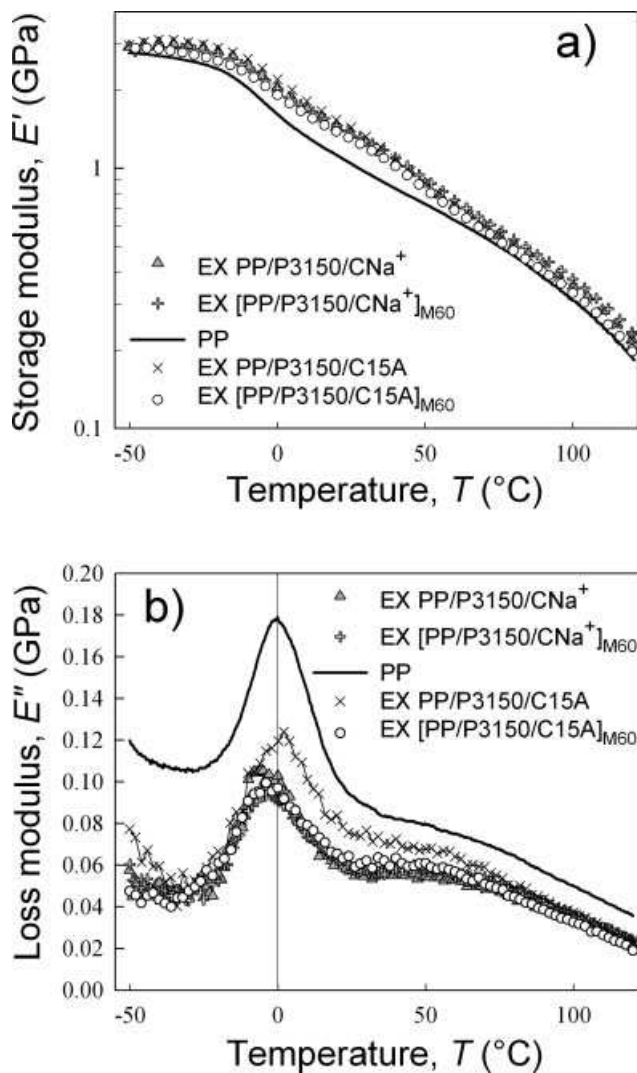
FIG. 16. Dynamic mechanical behavior of the following compounds in function of temperature: EX PP/P3150/CNa$^+$, EX PP/P3150/C15A, EX [PP/P3150/CNa$^+$]$_{M60}$, and EX [PP/P3150/C15A]$_{M60}$. (a) Storage modulus and (b) loss modulus.

efficient enough to prevent the aggregation of delaminated clay platelets in EX [PP/P3150/C15A]$_{M60}$, showing the same behavior as EX [PP/C15A]$_{M60}$.

Dynamic Mechanical Properties. Dynamic mechanical behavior of the compounds is shown in Fig. 16 presenting storage modulus (E') and loss modulus (E'') as a function of temperature from $-50°C$ to $120°C$. Liu and Wu [32] have demonstrated higher values of E' and E'' for PNC compounds in comparison with neat PP. In the same comparison, they also reported smaller values of T_g for these compounds increasing with clay content.

As shown in Fig. 16a, the storage modulus curves display significant increase for all PNC compounds in comparison with that of PP. The E' curves of EX PP/P3150/CNa$^+$ and EX [PP/P3150/CNa$^+$]$_{M60}$ are very similar; that of EX PP/P3150/C15A is higher than all the compounds and that of EX [PP/P3150/C15A]$_{M60}$ is the lowest one.

Despite the very different microstructure observed in these materials, their dynamic mechanical behavior is very similar (for example, at $T = 20°C$, 1.45 compared with 1.46 GPa for EX PP/P3150/CNa$^+$ and EX [PP/P3150/CNa$^+$]$_{M60}$, and 1.54 compared with 1.38 GPa for EX PP/P3150/C15A and EX [PP/P3150/C15A]$_{M60}$, respectively). Note that in the case of PP-based PNC, the changes in the crystallinity and the crystalline phase of PP are much more affected by the processing conditions and formulations (addition of coupling agent and clay) than by the clay dispersion itself, as it is the case for polyamide. As shown in a previous paper [33], the degree of crystallinity is not significantly affected by very different clay dispersions neither the crystalline phase.

As shown in Fig. 16b, one can note that the T_g of all shown compounds except that of EX PP/P3150/C15A is decreased in comparison with PP, as reported by Liu and Wu [32]. Seyhan et al. [34] reported an increase of T_g for the PNC compounds with carbon nanotubes. They explained this behavior by the decrease of polymer matrix mobility around the nanoparticles. The higher value of T_g for EX PP/P3150/C15A can be due to the stronger interaction between the organoclay particles and the matrix at the interface. This interaction is much smaller in the case of CNa$^+$-based compounds, because of the hydrophilic nature of inorganic clay. In the case of EX [PP/P3150/C15A]$_{M60}$, poor interaction between matrix and particles is suggested, which can be due to the inefficiency of the coupling agent (high M_w and low MA content) after ball milling.

CONCLUSIONS

In this work, the potential of ball milling was investigated in the melt-processing of PP/clay-based compounds to improve the clay dispersion. The microstructure analysis was coupled with rheological and dynamic mechanical characterization to study the effect of preliminary ball milling of clay alone, clay and coupling agent, and clay, coupling agent, and PP. The rheological behavior at low frequency of the PNC is in good agreement with the microstructure observations and is a good complementary characterization to study the effect of interactions between clay and matrix.

Depending on the milling parameters, the nature of the clay and the presence of other components during milling, different changes in the clay structure, such as delamination and breakage, have been observed. Nevertheless, the main concern is the particle agglomeration caused by milling. Preliminary milling of clay alone leads to large particle agglomeration in the case of the organoclay, resulting in a poor clay dispersion in the final compounds. Less agglomeration is observed for inorganic clay after ball milling. However, to keep the platelets delaminated after milling, the bare surface of clay should immediately react with macromolecule chains (e.g., coupling agent chains). By adding coupling agent in the preliminary mill-

ing of inorganic clay, different clay dispersion have been obtained depending on the type of coupling agent. An adequate polymeric chain like Epolene E43, with low molecular weight and higher amount of MA grafting, is a good choice to prevent clay agglomeration caused by milling and promote final clay dispersion improvement. The milling of clay with coupling agent and PP also improves greatly the dispersion of inorganic clay. Moreover, in the case of organoclay, a disordered clay structure with locally partial exfoliation has been observed.

Ball milling demonstrates some potential to improve the dispersion of the clay, specially in the case of the inorganic clays, which can be an alternative to the use of organoclays. However, this needs more optimization in milling conditions and efficiency in compounding.

ACKNOWLEDGMENTS

REFERENCES

1. S. Sinha Ray and M. Okamoto, *Prog. Polym. Sci.*, **28**, 1539 (2003).

2. L.A. Utracki, *Clay-Containing Polymeric Nanocomposites*, RAPRA, Shawbury, UK (2004).

3. S. Yariv and I. Lapides, *J. Mater. Synth. Process.*, **8**, 223 (2000).

4. E. Kasai, H. Mimura, K. Sugiyama, F. Saito, K. Akiba, and Y. Waseda, *Adv. Powder Technol.*, **5**, 189 (1994).

5. B. Cícel and G. Kranz, *Clay Miner.*, **16**, 151 (1981).

6. I. Sondi, M. Stubicar, and V. Pravdic, *Colloids Surf. A Physicochem. Eng. Asp.*, **127**, 141 (1997).

7. F. Dellisanti and G. Valdré, *Appl. Clay Sci.*, **28**, 233 (2005).

8. H.-J. Lu, G.-Z. Liang, X.-Y. Ma, B.-Y. Zhang, and X.-B. Chen, *Polym. Int.*, **53**, 1545 (2004).

9. C.M. Koo, H.T. Ham, M.H. Choi, S.O. Kim, and I.J. Chung, *Polymer*, **44**, 681 (2003).

10. W.H. Ruan, M.Q. Zhang, M.Z. Rong, and K. Friedrich, *Polym. Polym. Compos.*, **12**, 257 (2004).

11. W. Shao, Q. Wang, Y. Chen, and Y. Gu, *Mater. Manuf. Process.*, **21**, 173 (2006).

12. W. Shao, Q. Wang, F. Wang, and Y. Chen, *J. Polym. Sci.: Part B: Polym Phys.*, **44**, 249 (2006).

13. P. Mangiacapra, G. Gorrasi, A. Sorrentino, and V. Vittoria, *Carbohydr. Polym.*, **64**, 516 (2006).

14. M. Sepehr, L.A. Utracki, X.X. Zheng, and C.A. Wilkie, *Polymer*, **46**, 11557 (2005).

15. W.L. Bragg, *Proc. Camb. Phil. Soc.*, **17**, 43 (1913).

16. R.A. Vaia and E.P. Giannelis, *Macromolecules*, **30**, 8000 (1997).

17. S. Brunauer, P.H. Emmett, and E. Teller, *J. Am. Chem. Soc.*, **60**, 309 (1938).

18. R.H. Olley and D.C. Bassett, *Polymer*, **23**, 1707 (1982).

19. E.F. Aglietti, *Appl. Clay Sci.*, **9**, 139 (1994).

20. G. Suraj, C.S.P. Iyer, S. Rugmini, and M. Lalithambika, *Appl. Clay Sci.*, **12**, 111 (1997).

21. W. Xie, Z. Gao, W.-P. Pan, D. Hunter, A. Singh, and R. Vaia, *Chem. Mater.*, **13**, 2979 (2001).

22. J. Cervantes-Uc, J.V. Cauich-Rodríguez, H. Vázquez-Torres, L.F. Garfias-Mesías, and D.R. Paul, *Thermochim. Acta*, **457**, 92 (2007).

23. G. Edwards, P. Halley, G. Kerven, and D. Martin, *Thermochim. Acta*, **429**, 13 (2005).

24. N.G. Gaylord and M.K. Mishra, *J. Polym. Sci. Polym. Lett. Ed.*, **21**, 23 (1983).

25. R. Rengarajan, V.R. Parameswaran, S. Lee, M. Vicic, and P.L. Renaldi, *Polymer*, **31**, 1703 (1990).

26. S.J. Sinha Ray, *Ind. Eng. Chem.*, **12**, 811 (2006).

27. F.R. Costa, U. Wangenknecht, D. Jehnichen, M.A. Goad, and G. Heinrich, *Polymer*, **47**, 1649 (2006).

28. P.J. Carreau, D.C.R. De Kee, and R.P. Chhabra, *Rheology of Polymeric Systems Principles and Applications*. Hanser/ Gardner Publications, Cincinnati (1997).

29. J.D. Ferry, *Viscoelastic Properties of Polymers*, *3rd ed.*, Wiley, New York (1980).

30. M.J. Solomon, A.S. Almusallam, K.F. Seefelt, P. Somwangthanaroj, and P. Varadan, *Macromolecules*, **34**, 1864 (2001).

31. J. Ren, A.S. Silva, and R. Krishnamoorti, *Macromolecules*, **33**, 3739 (2000).

32. X. Liu and Q. Wu, *Polymer*, **42**, 10013 (2001).

33. F. Perrin-Sarazin, M.-T. Ton-That, M.N. Bureau, and J. Denault, *Polymer*, **46**, 11624 (2005).

34. A.T. Seyhan, F.H. Gojny, M. Tanoğlu, and K. Schulte, *Eur. Polym. J.*, **43**, 2836 (2007).